Transient Distribution of Magnetic Flux in DC Motor

By

Tsuguo ANDO* and Juro UMOTO*

(Received March 10, 1981)

Abstract

We introduce a numerical calculation considering the nonlinearity of the permeability of iron cores for a transient response of the magnetic flux to an abrupt change of the armature current at the speed control of the dc motor. From the calculated and measured results of the transient response, it is made clear that the transient response is greatly influenced by the conductivity of the yoke. Also, from many calculated results of the time behavior of the flux distribution, it is seen that the flux concentration near the inner surface of the yoke is caused by the eddy current in the yoke, and that the armature slots have a fairly large influence on the flux distribution on the armature surface.

1. Introduction

A direct current(dc) motor is widely applied to precise variable speed machines, servomechanism, etc., since it has a better speed-torque characteristic than an alternating current(ac) motor. However, at the speed control of the dc motor, a rapid change of the armature current occurs. It thus brings about a delay on the transient response of the magnetic flux in the dc motor and disturbs the regular distribution of the flux. This disturbance has a bad influence on the speed-torque characteristic, the commutation one, etc. Therefore, it is very important to analyse the transient response of the magnetic flux in the dc motor. Especially, in the commutating zone where the armature coils are short-circuited and an armature current alternates, the flux response is important. This is because a commutation spark may occur when a disturbance of the flux due to the change of the armature current is not overcome by the interpole flux excited by the interpole winding current.

Now, in large-sized dc motors, laminated cores are used not only for the armature, main pole and interpole, but also for the yoke, in order to decrease an eddy current which delays the transient response of the interpole flux. On the

* Department of Electrical Engineering.

other hand, in small-sized motors, the yoke is usually constructed with solid core for economical and industrical reasons.

Many studies on the transient response of the interpole flux in small-sized motors were reported, Those studies were mostly carried out on the assumption that the magnetic circuit in the dc motor can be simulated by a simple equivalent one with some constant permeability[1)-5)]. However, the actual dc motor has iron cores with a nonlinear permeability and a complex construction. Correspondingly, in order to analyse the flux response accurately, it is necessary to investigate the time behaviors of the flux distribution in the actual complex cross-section of the dc motor by using the two- or three-dimensional nonlinear theory considering the nonlinearity of the permeability of the iron cores.

In this paper, we first introduce some two-dimensional fundamental nonlinear equations to analyse the transient response of the magnetic flux in the dc motor. Then, we develop a numerical calculation for solving those equations, in which the nodal method considering Ampere's circuital law and the Crank-Nicolson method for the time derivative are used. Next, applying the method to an actual small-sized motor, we examine the transient response of the magnetic flux in the interpole, the variation of the flux distribution in the motor, etc. which occurred by the rapid change of the armature current.

2. Two-Dimensional Nodal Method for Numerical Solution of Magnetic Flux Distribution in DC Motor

2.1 Fundamental equations

The transient response of the magnetic flux in a dc motor can be described by solving the following Maxwell equations

$$\text{rot } \boldsymbol{H} = \boldsymbol{J}, \quad \text{rot } \boldsymbol{E} = -\frac{\partial \boldsymbol{B}}{\partial t}, \quad \text{div } \boldsymbol{B} = 0, \tag{1}$$

and the additional relations

$$\boldsymbol{B} = \mu \boldsymbol{H}, \quad \boldsymbol{J} = \boldsymbol{J}_s + \sigma \boldsymbol{E}. \tag{2}$$

In the equations, $\boldsymbol{H}$, $\boldsymbol{B}$, $\boldsymbol{E}$, μ and σ are the magnetic field intensity, the magnetic flux density, the electric field intensity, the permeability and the conductivity, respectively. $\boldsymbol{J}$ and $\boldsymbol{J}_s$ are the current densities which are induced in the iron cores and supplied to the winding conductor, respectively. Here, we assume that an eddy current induced in the conductor is negligible compared with $\boldsymbol{J}_s$. Now, by using the magnetic vector potential $\boldsymbol{A}$ and the electric scalar potential ϕ which satisfy $\boldsymbol{B}=\text{rot } \boldsymbol{A}$ and $\boldsymbol{E}=-\partial \boldsymbol{A}/\partial t-\text{grad } \phi$, Eqs. (1) and (2) can be trans-

formed to the equations with respect to $\boldsymbol{A}$, ϕ and $\boldsymbol{J}_s$. The analysis of the flux performance by these equations has been already done[6]. Here, imposing the supplemental condition div $\boldsymbol{A}=0$ upon $\boldsymbol{A}$, we can get $\phi=0$, and then we can analyse the response of the magnetic flux by the following equations

$$\left.\begin{aligned} &\text{rot } \boldsymbol{H}=\boldsymbol{J}_s-\sigma\partial\boldsymbol{A}/\partial t, \quad \text{div } \boldsymbol{A}=0,\\ &\boldsymbol{B}=\text{rot } \boldsymbol{A}, \quad \boldsymbol{H}=\nu\boldsymbol{B}, \end{aligned}\right\} \tag{3}$$

where $\nu=1/\mu$ is the reciprocal permeability.

For simplifying the analysis, let us assume that the axial length of the motor is sufficiently long and that the magnetic field does not vary in the axial direction (z direction). Then, Eqs. (3) are reduced to the following two-dimensional equations[7]

$$\left.\begin{aligned} &\text{rot } \boldsymbol{H}=\boldsymbol{k}\left(\frac{\partial H_x}{\partial y}-\frac{\partial H_y}{\partial x}\right)=\boldsymbol{k}\left(J_s-\sigma\frac{\partial A}{\partial t}\right),\\ &B_x=\frac{\partial A}{\partial y}, \quad B_y=-\frac{\partial A}{\partial x}, \quad H_x=\nu B_x, \quad H_y=\nu B_y, \end{aligned}\right\} \tag{4}$$

in the cross-section (x—y plane) of the motor perpendicular to the z direction. In these equations, $\boldsymbol{k}$ is the fundamental unit vector in the z direction, $A=A(x, y, t)$ and J_s are z components of $\boldsymbol{A}$ and $\boldsymbol{J}_s$, respectively, and B_x, H_x, B_y and H_y are x and y components of $\boldsymbol{B}$ and $\boldsymbol{H}$, respectively. In this connection, if the magnetic core has an anisotropic permeability, H_x and H_y in Eqs. (4) are rewritten by $H_x=\nu_x B_x$, $H_y=\nu_y B_y$, where ν_x and ν_y are x and y components of ν.

2.2 Nodal method

The finite difference or the finite element method has been mainly used to obtain an approximate numerical solution of Eqs. (4) under some given boundary conditions. Here, we introduce a nodal method derived by combining the finite difference and the finite element methods, where the former can give discrete equations which simulate Ampere's circuital law, and the latter can be easily applied to the complex field region as in the dc motor.

Figure 1 shows a half pole-pitch region of the cross-section of the dc motor, which is studied in this paper. That is subdivided into many triangular elements as shown in Fig. 2. Let us introduce the nodal method in the case where the vector potential in each element is expressed by a first order function of a position.

Now, in a triangular element e with nodes i, j and k in Fig. 3, the vector potential is assumed to be given by a linear approximation as follows:

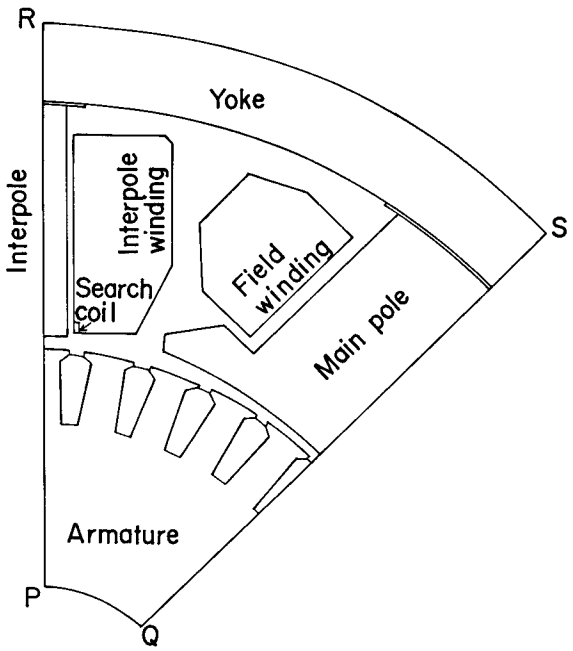

Fig. 1. Cross-sectional view of half pole-pitch of dc motor.

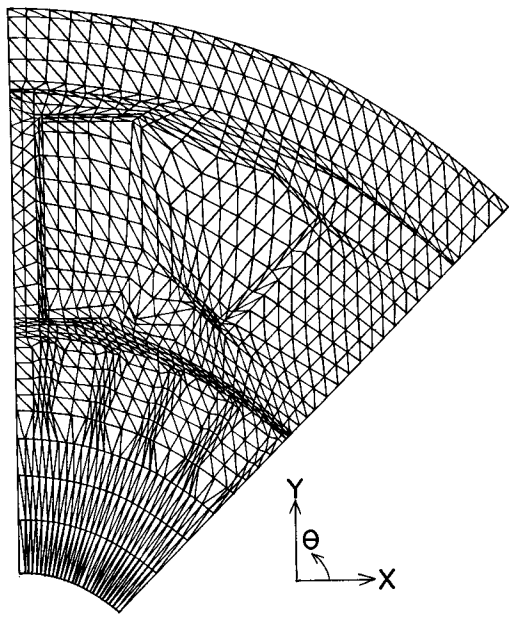

Fig. 2. Mesh of triangles for nodal method.

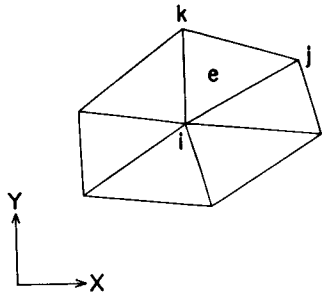

Fig. 3. Node i and its adjoining region.

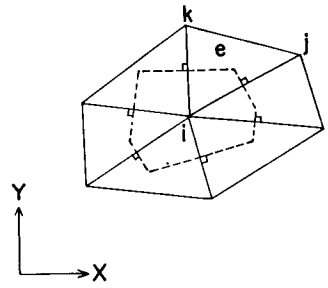

Fig. 4. Orthogonal grid in conventional nodal method.

$$A_e = a_e + b_e x + c_e y \,, \tag{5}$$

where

$$\left.\begin{aligned} &\begin{pmatrix} a_e \\ b_e \\ c_e \end{pmatrix} = \frac{1}{D_e}\begin{pmatrix} a_{ei} & a_{ej} & a_{ek} \\ b_{ei} & b_{ej} & b_{ek} \\ c_{ei} & c_{ej} & c_{ek} \end{pmatrix}\begin{pmatrix} A_i \\ A_j \\ A_k \end{pmatrix} \\ &a_{ei} = x_j y_k - x_k y_j,\ b_{ei} = y_j - y_k,\ c_{ei} = x_k - x_j,\ \text{etc.}, \\ &D_e = a_{ei} + a_{ej} + a_{ek} \,, \\ &A_m, x_m, y_m\text{: } A, x, y \text{ at node } m \,, \\ &m = i, j, k \,. \end{aligned}\right\} \tag{5}'$$

When it is assumed that the vector potential in every element is given by the same expression as Eq. (5), the normal component of $\boldsymbol{B}$ is continuous across a boundary line of two adjoining elements. On the other hand, the tangential component of $\boldsymbol{H}$ is not continuous, which is contrary to physical law. The nodal method is a superior numerical calculation, in which the boundary condition for $\boldsymbol{H}$ is replaced by Ampere's circuital law

$$\oint_c \boldsymbol{H}\cdot d\boldsymbol{l} = \int_S \boldsymbol{k}\left(J_s - \sigma\frac{\partial A}{\partial t}\right)\cdot d\boldsymbol{S} \tag{6}$$

around each node.

Next, let us derive a discrete nodal equation for node i by using Eq. (6). From Eqs. (4) and (5), the x components B_{ex} and H_{ex} and the y components B_{ey} and H_{ey} of $\boldsymbol{B}$ and $\boldsymbol{H}$ in element e are derived as follows:

$$\left.\begin{aligned} B_{ex} &= \frac{1}{D_e}\sum_m c_{em}A_m \,, \qquad B_{ey} = -\frac{1}{D_e}\sum_m b_{em}A_m \,, \\ H_{ex} &= \frac{\nu_e}{D_e}\sum_m c_{em}A_m \,, \qquad H_{ey} = -\frac{\nu_e}{D_e}\sum_m b_{em}A_m \,, \end{aligned}\right\} \tag{7}$$

where it is assumed that ν_e is expressed by the following Flöhlich formula

$$\nu_e = \frac{\eta_e}{1-\xi_e B_e}, \tag{8}$$

in which $B_e=(B_{ex}^2+B_{ey}^2)^{1/2}$, and η_e and ξ_e are the coefficients determined by the magnetization curve of the material in element e. From Eqs. (6) and (7), we can now obtain

$$\int_j^k \boldsymbol{H}\cdot d\boldsymbol{l} = \frac{\nu_e}{D_e}\sum_m (c_{ei}c_{em}A_m+b_{ei}b_{em}A_m), \tag{9}$$

$$\int_{S_e} \boldsymbol{k}J_s\cdot d\boldsymbol{S} = J_{se}S_e, \tag{10}$$

$$\int_{S_e} \boldsymbol{k}\sigma\frac{\partial A}{\partial t}\cdot d\boldsymbol{S} = \frac{\sigma_e S_e}{3}\frac{\partial}{\partial t}(A_i+A_j+A_k), \tag{11}$$

where J_{se} and σ_e are the values of J_s and σ, respectively, in element e, and $S=S_e=|D_e|/2$ is the area of element e. When Eq. (11) is used in the following formulation of the nodal equation, it is too difficult to get a convergence of the solution, because the mutual time coupling among the adjoining nodes i, j and k is too strong. Accordingly, we use the following approximate expression

$$\int_{S_e} \boldsymbol{k}\sigma\frac{\partial A}{\partial t}\cdot d\boldsymbol{S} = \sigma_e S_e\frac{\partial A_i}{\partial t} \tag{12}$$

instead of Eq. (11). By spreading the integral region in Eqs. (9), (10) and (12) to the whole region shown in Fig. 3, and completing Ampere's circuital law around node i, the nodal equation is established as the following expression

$$f_i = s_i-\frac{\partial g_i}{\partial t}, \tag{13}$$

where f_i, s_i and g_i are the functions which are derived from $\oint_c \boldsymbol{H}\cdot d\boldsymbol{l}$, $\int_S \boldsymbol{k}J_s\cdot d\boldsymbol{S}$ and $\int_S \boldsymbol{k}\sigma A\cdot d\boldsymbol{S}$, respectively. In this connection, in the conventional nodal method[8], they carried out the integrations in Eq. (6) in the region surrounded by broken lines as shown in Fig. 4. The process of the above conventional integration becomes complicated, and also each element must be an acute-angled triangle.

In Eq. (13), there is contained the time derivative $\partial g_i/\partial t$ of g_i. Therefore, in order to numerically solve the equation, we apply Crank-Nikolson's finite difference method to $\partial g_i/\partial t$, by which a sufficiently accurate approximate value of a time derivative can be obtained[9]. When the value of g_i at $t=t$ is evaluated, the value at $t=t+\Delta t$ is given by the following equation

$$(g_i)_{t=t+\Delta t} = (g_i)_{t=t}+\Delta t\left\{\varepsilon\left(\frac{\partial g_i}{\partial t}\right)_{t=t+\Delta t}+(1-\varepsilon)\left(\frac{\partial g_i}{\partial t}\right)_{t=t}\right\} \tag{14}$$

where ε is a weight factor of the time derivative and $0\leq\varepsilon\leq 1$. By substituting Eq. (13) into Eq. (14), we get

$$(g_i+\varepsilon\Delta t f_i)_{t=t+\Delta t} = \{g_i-(1-\varepsilon)\Delta t(f_i-s_i)\}_{t=t}+\varepsilon\Delta t(s_i)_{t=t+\Delta t}\,. \tag{15}$$

This is the final form of a discrete nodal equation for node i, in which $\varepsilon=1$ for node of $g_i=0$.

Here, let us consider the nodal equtaion for node i which exists on the boundaries. On a boundary where the normal component B_n of $\boldsymbol{B}$ is zero, $A=A_i$ is constant, and we can state $f_i=A_i$, $s_i=$constant and $g_i=0$ in Eq. (13). On another boundary where $\boldsymbol{B}$ has only a normal component, $\partial A/\partial n=0$ is satisfied. Hence, the nodal equation given by Eq. (13), which is derived from integrating Eq. (6) in an incomplete circulating integral region, satisfies $\partial A/\partial n=0$.

Finally, from Eq. (15) and the boundary conditions, the nonlinear simultaneous nodal equations for all nodes in Fig. 2 are expressed as follows:

$$(\boldsymbol{G}+\varepsilon\Delta t\boldsymbol{F})_{t=t+\Delta t} = \{\boldsymbol{G}-(1-\varepsilon)\Delta t(\boldsymbol{F}-\boldsymbol{S})\}_{t=t}+\varepsilon\Delta t(\boldsymbol{S})_{t=t+\Delta t}\,, \tag{16}$$

in matrix form, where

$\boldsymbol{F}$: a nonlinear and sparse matrix constructed with f_i,

$\boldsymbol{G}$: a row matrix constructed with g_i,

$\boldsymbol{S}$: a row matrix constructed with s_i.

By solving numerically Eqs. (16), the transient value of A at each node is obtained, and subsequently the transient response and distribution of the magnetic flux, etc. can be calculated. For numerically solving Eqs. (16), an iterative procedure is needed. By using the successive relaxation method, repetition times can be fairly decreased.

3. Calculation Results and Discussions

3.1 Numerical conditions

We apply our numerical calculation to the dc motor with the following specifications:

number of poles: 4, output: 3.7 *kW*, speed: 400 *rpm*, terminal voltage: 440 *V*, armature current: 9.8 *A*, number of armature circuits: 2, number of armature slots: 37, number of conductors per slot: 64, number of segments: 185, number of turns of interpole winding per pole: 173, the same for field winding per pole: 1600, outside diameter of armature: 0.241 m, the same

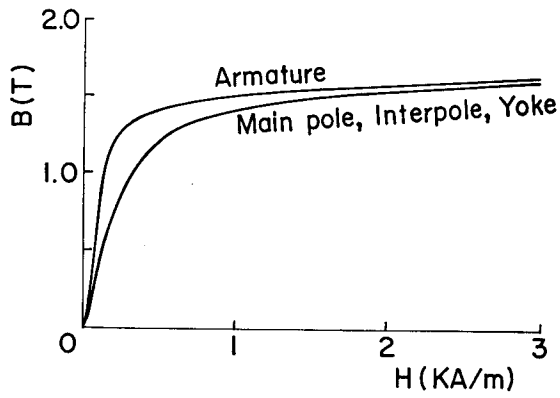

Fig. 5. Magnetization curves.

for yoke: 0.455 *m*, width, hight and length of interpole: 0.016, 0.075, 0.140 *m*, the same for main pole: 0.076, 0.077, 0.147 *m*.

The magnetization curve of the armature, main pole, interpole and yoke cores are indicated in Fig. 5. For simplifying the digital computation and yet obtaining sufficiently accurate solutions, we assumed the following:

(1) The armature stands still at the position shown in Fig. 1, because a numerical analysis is too difficult when the relative position between the armature and the stator is varying.

(2) The number of 37 slots is approximated by 36 for obtaining the symmetricity of the cross-section of the motor as shown in Fig. 1.

(3) The current density in the slot which keeps the armature coils short-circuited by the brushes is estimated as a half of that in the other slots.

(4) Neglecting the leakage fluxes from the outer surface of the yoke and the inner surface of the armature, we put $A=0$ on the boundaries PQ and RS in Fig. 1.

(5) In the armature, main pole and interpole constructed with laminated cores, the conductivity $\sigma=0$. In the yoke of a solid silicon steel core, $\sigma=0$, 2 or 5 *MS/m*, by which the influence of σ on the transient response of the magnetic flux is investigated.

3.2 Calculation results and discussions

In Fig. 6, there is shown the transient response of the flux ϕ through the search coil in the lower part of the interpole winding in the case where the current $I_a=8\{1-\exp(-t/0.00525)\}A$ is applied to the armature and interpole circuits. In the figure, ϕ is normalized by ϕ_∞ which is the linkage flux at $t=\infty$ when an eddy current induced in the yoke vanishes, i.e. in the steady state. The experi-

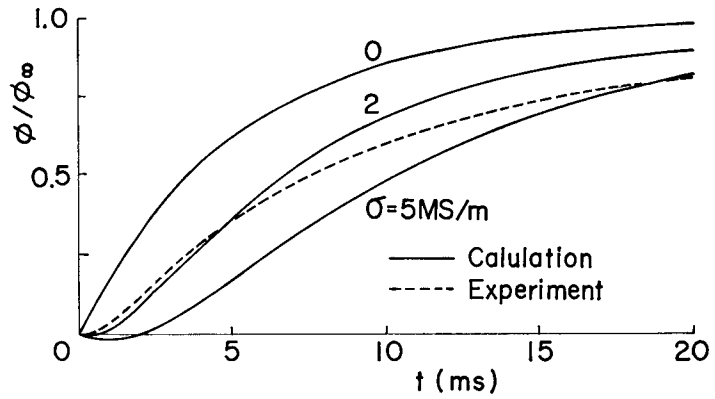

Fig. 6. Transient response of magnetic flux interlinking with search coil in interpole.

mental result was obtained by integrating the induced electromotive force in the search coil. The figure shows that the conductivity of the yoke has remarkable influence on the transient response of the interpole flux.

In Figs. 7, 8 and 9, caluculated flux distributions at $t=1$, 5 and 10 *ms* are shown for $\sigma=0$, 2 and 5 *MS/m*, respectively, and in Fig. 10 the same for the steady state. In these figures, ΔA is a contour interval of A between neighbouring equi-vector potential lines, that is flux lines. It is proportional to the flux in the inter-

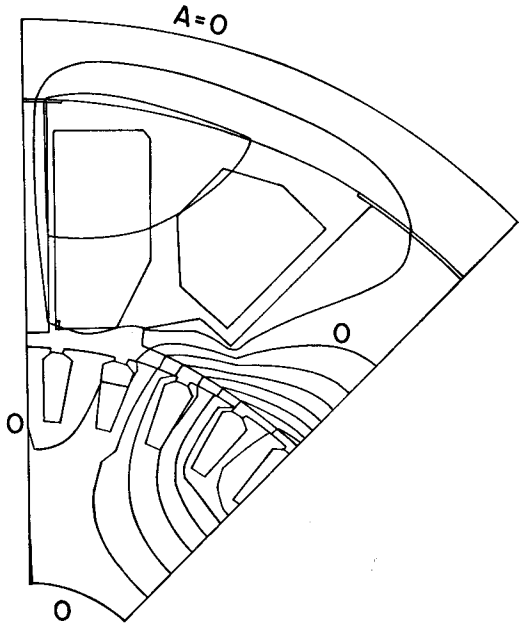

(a)

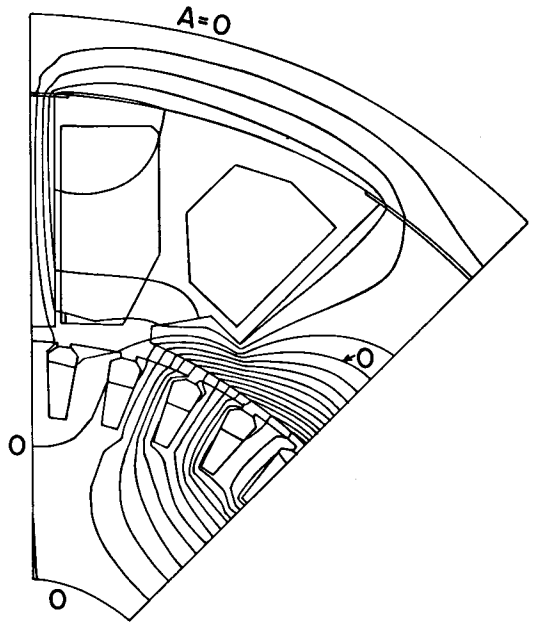

(b)

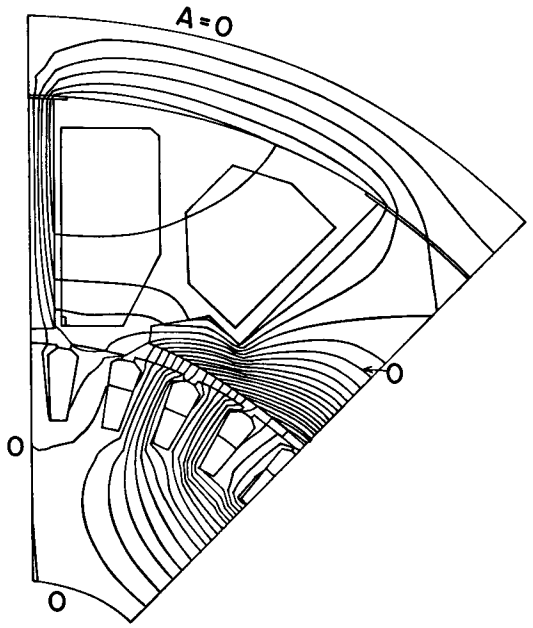

(c)

Fig. 7. Flux distributions for $\sigma=0$.
(a) $t=1$ *ms* and $\Delta A=0.25$ *mWb/m*.
(b) $t=5$ *ms* and $\Delta A=0.5$ *mWb/m*.
(c) $t=10$ *ms* and $\Delta A=0.5$ *mWb/m*.

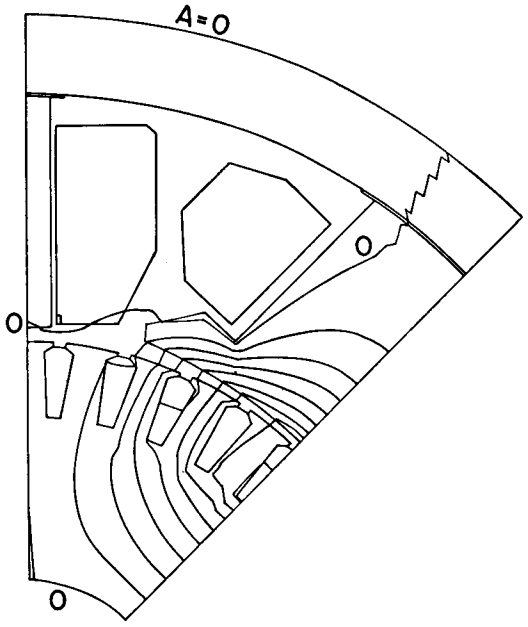

(a)

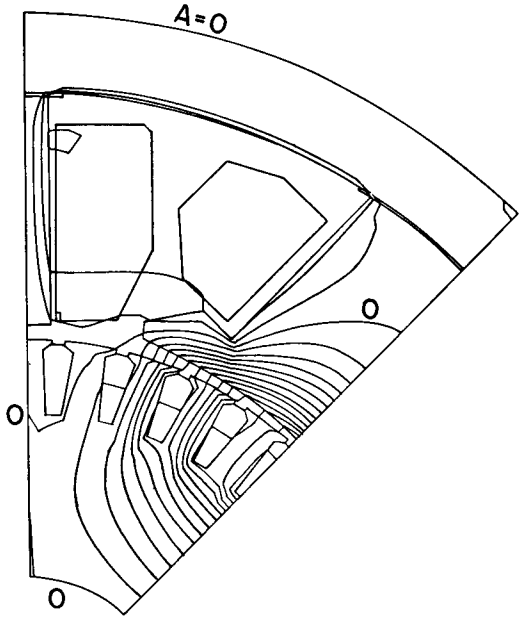

(b)

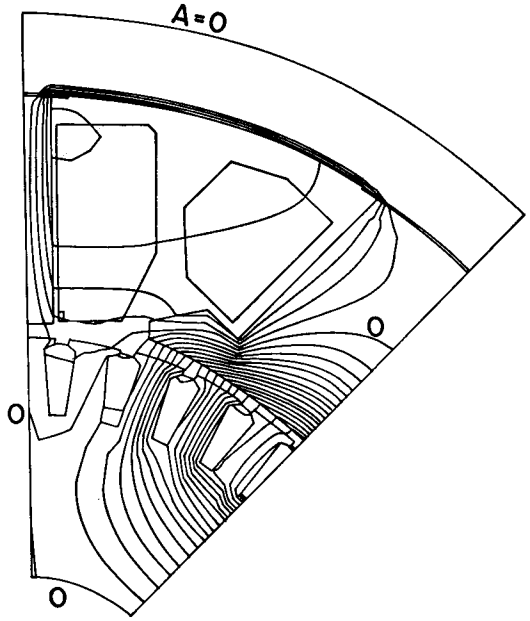

(c)

Fig. 8. Flux distributions for $\sigma=2$ *MS/m*.
(a) $t=1$ *ms* and $\Delta A=0.25$ *mWb/m*.
(b) $t=5$ *ms* and $\Delta A=0.5$ *mWb/m*.
(c) $t=10$ *ms* and $\Delta A=0.5$ *mWb/m*.

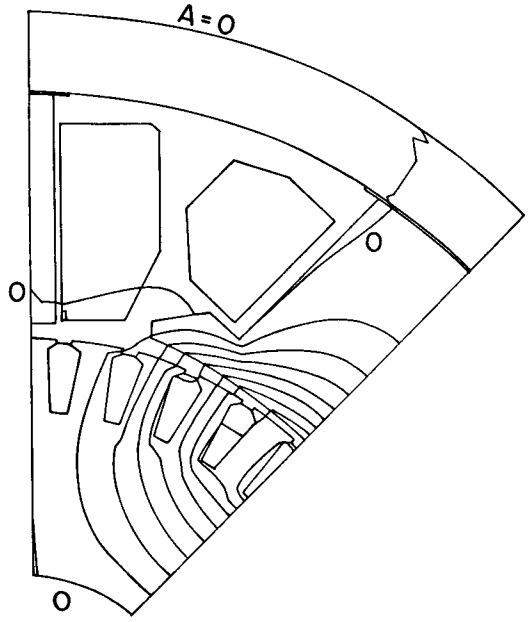

(a)

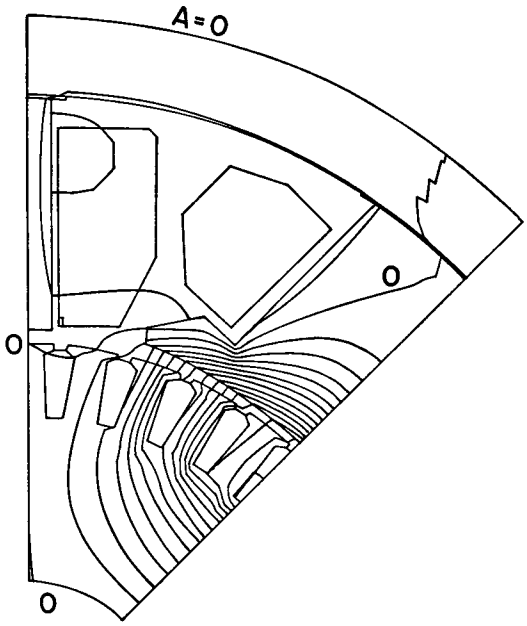

(b)

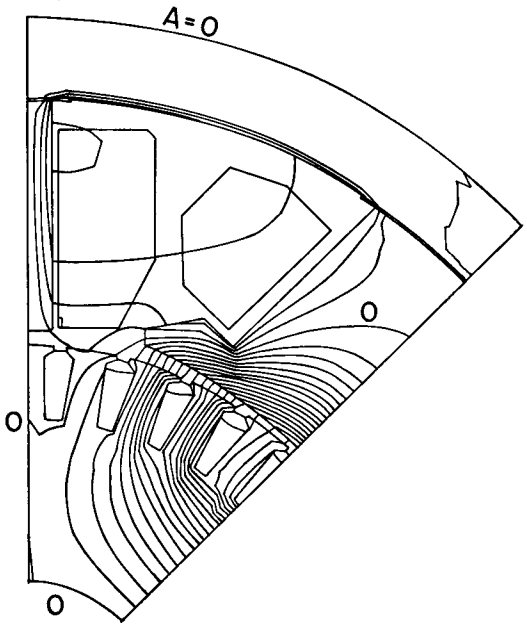

(c)

Fig. 9. Flux distributions for $\sigma=5$ *MS/m*.
(a) $t=1$ *ms* and $\Delta A=0.25$ *mWb/m*.
(b) $t=5$ *ms* and $\Delta A=0.5$ *mWb/m*.
(c) $t=10$ *ms* and $\Delta A=0.5$ *mWb/m*.

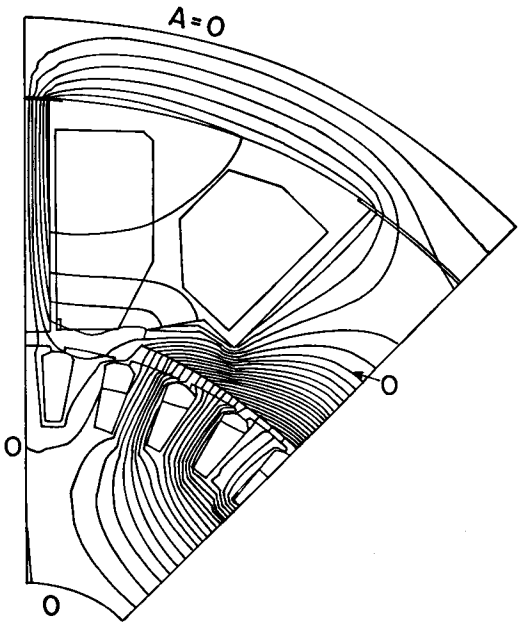

Fig. 10. Flux distribution in steady state for $I_a=8A$ and $\Delta A=0.5\ mWb/m$.

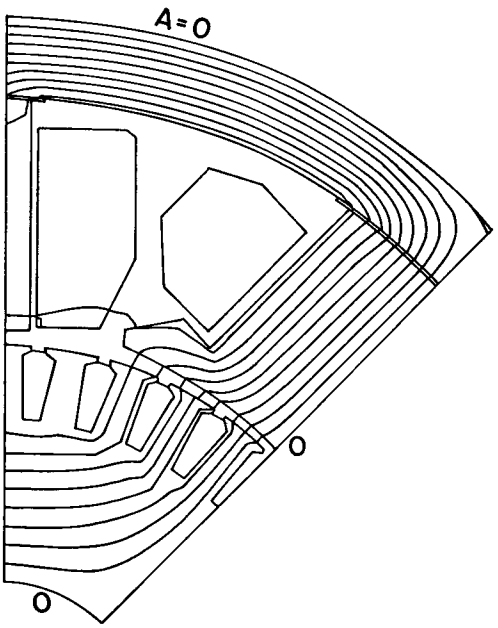

Fig. 11. Stationary distribution of magentic flux for applied field current $I_f=1.5\ A$ and $\Delta A=5\ mWb/m$.

val. From Fig. 7, for $\sigma=0$, we can see the movement of the flux which responds immediately to the variation of the current I_a. In Figs. 8 and 9 for fairly large values of σ, the flux in the yoke is apt to flow near the inner surface because of an induced eddy current[10]. In the slot under the interpole, the flux induced by the armature current appears without delay. It takes a fairly long time to negate the above flux with the one generated by the interpole current. Consequently, in order to obtain good commutation characteristics, we must consider a counter-plan such as laminating the yoke core or relaxing the change of the armature current.

Next, Fig. 11 shows the flux distribution in the steady state in the case where the constant field current $I_f=1.5\ A$ is applied to the main pole winding. Comparing Fig. 11 with Fig. 10, it is made clear that the magnetic flux which occurred by the field current is much more than that by the armature current.

Finally, the distribution of the radical component of the magnetic flux density on the outer surface of the armature is shown in Fig. 12. We can see that the armature slots have a fairly large influence on the flux distribution.

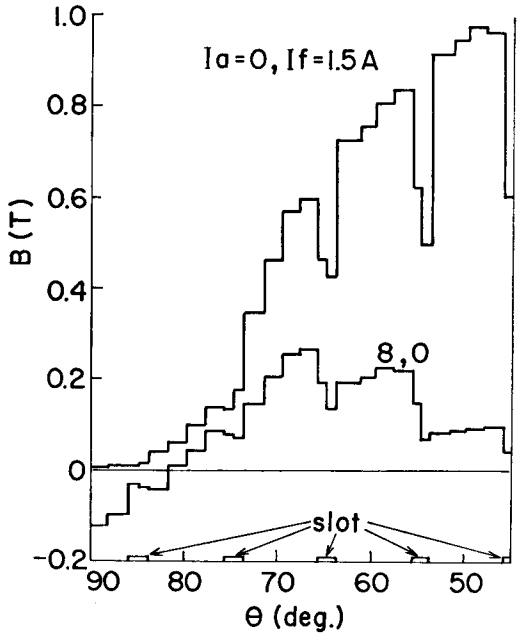

Fig. 12. Stationary distribution of radial component of magnetic flux density on armature surface.

4. Concluding Remarks

We introduced the two-dimensional theoretical equations, considering the

nonlinearity of the permeability of iron cores and the numerical solution for the transient distribution of the magnetic flux. This flux is varied by an abrupt change of the armature current at the speed control of the dc motor. From the calculated and measured results of the transient response, it was clarified that the transient response is greatly influenced by the conductivity of the yoke. Also, we could see from the calculated results of the time behavior of the flux distribution that the flux concentration near the inner surface of the yoke is caused by the eddy current in the yoke. Furthermore, it was seen that the armature slots have a fairly large influence on the flux distribution on the armature surface.

Acknowledgement

The authors wish to express their thanks to Professor H. Okitsu and Lecturer I. Morita of the Faculty of Engineering, Tokushima University, for their help in these experiments, and their offer of the dc motor specifications.

References

1) R. Rüdenberg: 'Transient Performance of Electric Power System', McGraw-Hill, Inc., New York, p106 (1950).
2) J. Švajcr: IEEE Trans. on Mag., **Mag-10**, 54 (1974).
3) Y. Matsushima, H. Fujiwara et al.: Technical Group. Rotating Machine. IEE. J. Japan, **RM-80-4** (1980).
4) L.V. Bewley: 'Two-Dimensional Fields in Electrical Engineering', Dover Publications, Inc., New York, p90 (1963).
5) I. Morita, H. Okitsu et al.: Convention Records. Annual Meeting. IEE. J. Japan, No. 704 (1980).
6) T. Nakata, N. Takahashi and Y. Kawase: Technical Group. Information Processing. IEE. J. Japan, **IP-80-49** (1980).
7) T. Ando and J. Umoto: Convention Records. Annual Meeting. IEE. J. Japan, No. 702 (1980).
8) A.Y. Hannalla and D.C. Macdonald: IEEE Trans. on Mag., **Mag-11**, 1544 (1975).
9) G.D. Smith (Translated by Y. Fujikawa): 'Numerical Solution of Partial Difference Equations', Sciencesha, Ltd., Japan, p17 (1977).
10) T. Ando and J. Umoto: Trans. IEE. Japan, **100-B** 492 (1980).